IEEE Access
Multidisciplinary ⋮ Rapid Review ⋮ Open Access Journal

Received 6 July 2023, accepted 28 August 2023, date of publication 6 September 2023, date of current version 13 September 2023.

Digital Object Identifier 10.1109/ACCESS.2023.3312564

RESEARCH ARTICLE

Autonomous Frequency Regulation Using Battery Energy Storage Systems of EV Charging Station

CHANGWOO YOON[1], (Member, IEEE), NGOC-DUC NGUYEN[1], YONG CHEOL KANG[2], (Senior Member, IEEE), AND YOUNG-IL LEE[1], (Senior Member, IEEE)

[1]RCEIT, Seoul National University of Science and Technology, Seoul 01811, South Korea
[2]School of Electronic and Electrical Engineering, Yonsei University, Seoul 03722, South Korea

Corresponding author: Young-Il Lee (yilee@seoultech.ac.kr)

This work was supported in part by the Basic Science Research Program through the National Research Foundation of Korea (NRF) funded by the Ministry of Education under Grant NRF-2019R1A6A1A03032119, and in part by the Korea Institute for Advancement of Technology (KIAT) through the International Cooperative Research and Development Program under Project P0017189.

ABSTRACT Increasing penetration of replenished renewable energy sources (RES) to the power grid is inevitable and brings stability challenges to traditional electric power systems (EPS). One of them is the frequency fluctuation due to the high participation of RES in the EPS. To reduce the grid frequency deviation, in this paper, an autonomous frequency regulation (FR) controller is proposed using the power of battery energy storage systems (BESS) in electric vehicle charging stations (EVCS) while providing the charging service. A proportional-integral (PI) controller scheme with a contribution factor is used in the proposed FR controller. The contribution factor determines the maximum power from BESS used for the proposed FR. The required power for the FR is then used to generate the setpoint for the inner-loop current controller of the grid-connected inverter (GCI). An impedance-based stability analysis considering the PI current controller and PLL gains for the LCL-filtered GCI is conducted. For the performance evaluation, the proposed FR controller is demonstrated in the IEEE 14-bus power system in PSCAD simulation.

INDEX TERMS Frequency regulation, battery energy storage system, random power load, grid service, renewable energy source.

I. INTRODUCTION

The diversification of electric vehicles (EV) is explosively increasing, and the demand for fast charging is also rapidly growing. However, the expansion of fast-charging facilities is not keeping up with the demand due to the current electricity tariff structure and power restrictions on the existing distribution network [1]. One solution is using the battery energy storage system (BESS) to limit the peaking electricity demand or to cooperate with nearby variable renewable energies (VREs) [2], [3], [4], [5], [6], [7]. These BESSs in rapid EV charging stations will be deployed over large areas, and if there are some BESSs resting, those unassigned resources may be utilized in the frequency regulation (FR) for the electric power system (EPS) flexibility enhancement [8], [9], [10].

The associate editor coordinating the review of this manuscript and approving it for publication was Shafi K. Khadem.

The conventional EPS frequency control scheme consists of primary frequency control (PFC), secondary frequency control (SFC) called automatic generation control (AGC), and tertiary frequency control [11], [12], [13]. PFC autonomously increases the output power proportional to the frequency deviation by deploying the PFC reserve if the frequency deviation exceeds the deadband of the governor of the synchronous generators. In contrast, to eliminate steady-state frequency errors either after PFC is terminated or under normal operation, AGC sends the incremental power to the individual online generators every four seconds. That is why it has a slow response time from tens of seconds to over 10 minutes [14]. Thus, AGC is generally not fast enough to respond to continuously varying loads, which causes large random frequency deviations from the nominal value under normal operation. This inevitably activates PFC if the frequency deviation goes over the ±36 mHz

band for the Korean EPS. As a result, the PFC reserve is deployed and thus the EPS frequency stability is unable to be secured until the PFC reserve is fully recovered [15]. In addition, the frequent PFC activation under normal operation results in the mechanical actuators aging of the governor.

BESSs, which use electrical energy stored in batteries, can provide a faster FR response and react to frequency deviations less than ±36 mHz, thereby reducing the number of primary control activations [16], [17], [18], [19], [20], [21]. Researches on FR using dedicated large-scale BESSs started since the last three decades ago [16], [17]. The advantages of the instantaneous power response of the BESS were presented in [16], but the dynamics and nonlinearities in the governor in the EPS such as the deadband, rate-limiters, and AGC were ignored. In [17], more detailed dynamics and the nonlinearities were considered, and a damping effect of the BESS on EPS frequency was described. The use of aggregated BESSs in the EPS for FR were studied by employing a centralized EPS controller while taking the BESS state of charge (SOC) into consideration in [8], [16], [17], [18], [19], [20], [21], [22], [23], and [24]. In [25], the limitations of the centralized controller to manage many distributed BESSs were addressed.

One of the tangible problems of the centralized controller is the computational burden of generating charge/discharge commands for the individual BESS. In [26], the BESS inside the traditional power plants was used to assist the AGC to reduce the frequency deviation while keeping the BESS degradation as small as possible in terms of SOC and DOD levels. This solution could not be cost-effective when the installation and operation cost of BESS inside the traditional generators is not covered by providing some local load services. The concept of commercial buildings is proposed in [27] to use the BESS inside the buildings for the FR service while charging the EV. Among the commercial buildings, the V2G function is enabled, and a number of BESS, including EV batteries, were used to compensate for the load demand variation. The high-frequency component of the load was effectively provided by the network of BESS resulting in a reduction of frequency deviation at each building. In this FR scheme, the primary and secondary frequency control signals are sent to the BESS, however, the effect of communication delay on the FR is not comprehensively provided. Therefore, an FR model for a large interconnected power system using various ESS considering the impact of the communication delay on the stability and ESS management was investigated in [28]. To avoid the communication delay, autonomous operation of BESSs for FR is gaining an attention [25], [29], [30], [31]. The FR performance degradation due to the delays that occur during the communication process was addressed in [25]. However, the scheme in [25] may not be called autonomous because it is still taking commands from the centralized controller. In addition, the frequency deviation threshold of ±100 mHz set in [25] has limitations to fully avoid the primary control activation under normal operation. In [30], the BESS controller is dedicated to the FR service, and it is not used for other charging tasks. The optimal control action of BESS is then presented while keeping BESS degradation to a minimum. In [29] and [31], the V2G function is the focus of the proposal for the smart grid. When the EVs are charged at home, a smart charging control is proposed to primarily satisfy the scheduled charging by the vehicle user while providing the FR service. The V2G function is a bi-directional power transfer, so this operation can harm the EV battery life. Therefore, in our proposed method, the BESS in the charging station is utilized for the FR, not the EV batteries. EV users only need to wait for a longer charging time when they agree to participate in the FR service without degrading their EV's battery life.

Another important aspect of autonomous operation is the frequency measurement method, but a proper phase-locked-loop (PLL) was not considered in [31]. In addition, the multitasking ability of the BESS is essential to achieve a higher economic viability. The FR function of the BESSs should be operable to the originally committed functions e.g., load shifting BESS, peak shaving BESS, uninterruptible power supply etc. to recruit various kinds of distributed autonomous BESSs.

This paper addresses the autonomous FR of the BESSs installed in the fast-electric vehicle charging stations (FEVCSs). The primary task of the BESSs is charging the electric vehicles (EVs) when EVs require energy. However, when the BESS is not fully occupied or in a retention mode, the BESS is able to participate in the autonomous FR to mitigate the frequency fluctuations under normal operation of the EPS. Unlike the research in [25], the proposed autonomous FR method uses no deadband and thus the frequency fluctuations can be significantly mitigated while forcing the frequency deviation within the governor deadband of the synchronous generators. As a result, the PFC activation is significantly avoided under normal operation, thereby maintaining the EPS frequency stability. The modified IEEE 14-bus system are used to investigate the performance of the proposed method. In the modified IEEE 14-bus system, six BESSs are installed in six distributed fast EV charging stations to support the charging EVs.

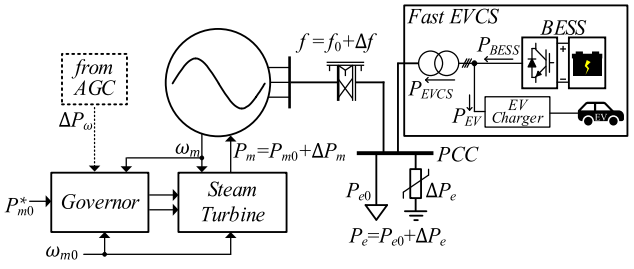

FIGURE 1. A simple EPS for the concept explanation.

II. PROPOSED FR METHOD FOR THE BESSs IN THE FEVCSs

This section describes the proposed autonomous FR method. FIGURE 1 shows the simple EPS that includes one steam-turbine synchronous generator and one FEVCS. The BESSs in the FEVCSs are primarily dedicated to charge the EVs. The frequency deviation (Δf) from the nominal frequency (f_0) is caused by the continuous load variation under normal operation of the EPS. Ignoring the losses in the transmission system, the power (P_m) delivered from the prime mover should be kept the same as the load (P_e) consisting of the varying load component (ΔP_e) and the fixed load (P_{e0}). If the average generator power input (P_m) and the average loading (P_e) are the same, and the frequency of the synchronous generator (ω_m) remains at the nominal value (ω_{m0}). However, since the aggregated load is continuously changing, the frequency can be kept at ω_{m0} only when the load fluctuations are compensated by adjusting P_m.

PFC and SFC have been used to adjust P_m. PFC is activated without any command signal from the EPS operator if Δf exceeds the deadband. As SFC, AGC sends a command signal (ΔP_ω) at every 4 s in the Korean EPS to eliminate Δf under normal operation. SFC is activated whenever Δf exists. Conversely, PFC is activated only when if Δf exceeds the deadband. Note that PFC is generally designed to arrest the frequency decline by deploying the PFC reserve following a frequency event such as generator trip.

Note that AGC through the synchronous generators is quite slow because it takes quite a long time to convert the fluid of steam into P_m through mechanical turbines and an AGC signal is issued at every 4 s. In addition, even aggregated load in the EPS varies too fast for a mechanical-based system to respond. Thus, Δf that always occurs is unable to be completely eliminated through AGC. Sometimes Δf can exceed the governor deadband, thereby deploying the PFC reserve. As a result, the EPS stability can be degraded.

In order to handle this frequency regulation issue, BESSs can participate in mitigating the frequency fluctuations either centrally or autonomously. In this paper, to achieve the higher frequency mitigating capability, an autonomous FR strategy using the distributed BESSs in FEVCSs without receiving the command signal from AGC will be presented.

By assuming that there exists a BESS in the FEVCS for EV charging support, the power relation at the charging station can be written as:

$$P_{\text{EVCS}} = P_{BESS} - P_{EV}, \tag{1}$$

where P_{EVCS} is the EVCS power injecting to the utility grid in FIGURE 2, P_{BESS} is the BESS power, and P_{EV} is the power used to charge the EV at the EVCS.

The BESS power P_{BESS} is physically constrained as:

$$P_{BESS}^{min} \le P_{\text{BESS}} \le P_{BESS}^{max} \tag{2}$$

where P_{BESS}^{max} and P_{BESS}^{min} are the maximum and the minimum power for the BESS, respectively and typically, $P_{BESS}^{min} = -P_{BESS}^{max}$.

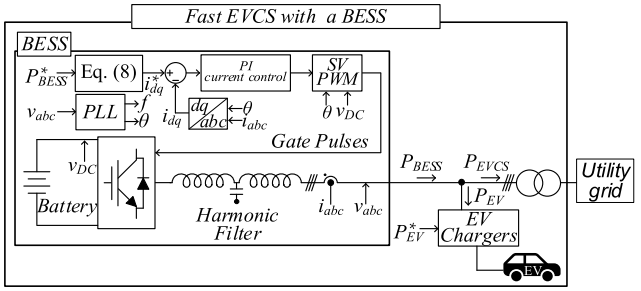

FIGURE 2. FEVCS with an assisting BESS.

Note that the reference for P_{EV} is generated from the EVs when the charging service starts, and its portions are determined by the energy management system (EMS) of the FEVCS as:

$$P_{EV}^{o} = P_{BESS}^{o} - P_{EVCS}^{o}, \tag{3}$$

where P_{EV}^{o}, P_{BESS}^{o} and P_{EVCS}^{o} represent the pre-computed reference for P_{EV}, P_{BESS} and P_{EVCS} by the EMS of EVCS, respectively. If the EVCS is not assigned for the FR service, then these pre-computed references will be the actual references. However, the EVCS is assumed to participate the FR service in this paper, so the actual reference for the BESS and EV will be determined by the following FR controller.

It is assumed that $P_{EV}^{o} > 0$, i.e. the vehicle-to-grid power transmission is not permitted. The FR controller to compensate for Δf is designed as:

$$P_{FR}(t) = K_{pFR} \cdot \Delta f(t) + K_{iFR} \cdot \int_0^t \Delta f(\tau)\, d\tau \tag{4}$$

where K_{pFR} and K_{iFR} represent the proportional and integral gains of the FR controller, respectively. Here, $\Delta f = f_o - \hat{f}$ has a mean value of zero, f_o is 60 Hz, and $\hat{f}$ is the estimated frequency using PLL. This FR operation will be bounded by

$$|P_{FR}| < \alpha . P_{BESS}^{max}, (0 < \alpha < 1), \tag{5}$$

where α is a contribution factor used to determine how much percentage of the BESS power will be assigned for the FR service.

Considering the physical constraint (2) and the required power for the FR service, the power references for P_{BESS} and P_{EV} will be modified as:

$$P_{BESS}^{*} = \begin{cases} P_{BESS}^{o} + P_{FR}(t), & if \ \left|P_{BESS}^{o} + P_{FR}(t)\right| < P_{BESS}^{max} \\ P_{BESS}^{max}, & otherwise, \end{cases} \tag{6}$$

and

$$P_{EV}^{*} = \begin{cases} P_{EV}^{o}, & if \ \left|P_{BESS}^{o} + P_{FR}(t)\right| < P_{BESS}^{max} \\ P_{BESS}^{max} - P_{FR}(t), & otherwise \end{cases} \tag{7}$$

Finally, the actual reference for BESS and EV are P_{BESS}^{*} and P_{EV}^{*} as defined in (6) and (7), respectively.

From (7), the EV charging operation could be altered by the FR operation when $P^{o}_{BESS} + P_{FR}(t)$ violates the physical limit of the BESS.

The operation mode of the BESS is expressed in two ways according to the polarity of P^{*}_{BESS}. In one mode, P_{EV} is partially or wholly supplied by the BESS ($P^{*}_{BESS} > 0$). In the other mode ($P^{*}_{BESS} \leq 0$), the BESS and the EV are charged from the grid.

The mean value of P_{FR} can be assumed to be zero because the integral action of AGC removes the frequency offset in Δf over the long period.

In FIGURE 2, a detailed diagram of the FEVCS is illustrated. As the main charging power is from the grid, an efficient DC/AC interfacing unit, an active front end converter are adopted, and P^{*}_{BESS} is made into P_{BESS} synchronized with the phase angle (θ) in a phase-locked-loop (PLL) [32]. The PLL uses the locally measured voltage v_{abc} and thus a communication signal from centralized controller is not required. To obtain the current reference for the synchronous reference frame (SRF) quantity (i^{*}_{dq}) a power to current conversion gain is calculated as,

$$\left\{ i^{*}_{d} = 0, i^{*}_{q} = \frac{\sqrt{2}}{\sqrt{3}} \frac{P^{*}_{BESS}}{rms\left(v_{ll,abc}\right)} \right\} \tag{8}$$

where $v_{ll,abc}$ is the line-to-line value of v_{abc} and $rms()$ is root mean square function.

The SRF quantity of the line current (i_{dq}) is converted from the phase current (i_{abc}) and an inner-loop PI current controller works to regulate i_{dq} to track i^{*}_{dq} in FIGURE 2. The output of the current controller is given to the space-vector pulse-width-modulator (SVPWM) to generate the corresponding gate pulses for switches. As a result, the battery power with the voltage (v_{DC}) is modulated and filtered to supply the exact amount of P_{BESS}.

Typically, the EV chargers in FEVCS receive upper power limits from all connected EVs and the chargers can decide how much power would be delivered depending on the EVCS power conditions. Therefore, P_{EV} can be reduced as (7) according to the FR conditions while providing the EV charging services, and finally it will track P^{*}_{EV} and decrease to zero when EVs is fully charged.

III. MODEL SYSTEM

As shown in FIGURE 3, the modified IEEE 14-bus system is chosen as the test system to investigate the performance of the proposed FR scheme based on a PSCAD simulator. Ten fluctuating loads are added in addition to the existing eleven fixed loads. The total load ranges from 250 MW to 260 MW under normal operations. The nominal bus voltage of the model system is 138 kV, and the RMS voltage used at the EVCS is 400 V using the step-down transformer as shown in FIGURE 2. The power ratings and inertia constants of the synchronous generators are defined in FIGURE 3, i.e. 120 MVA and H=4 s at Bus 2. Six BESSs (each 500 kW/500 kWh) are added to the IEEE 14-bus system

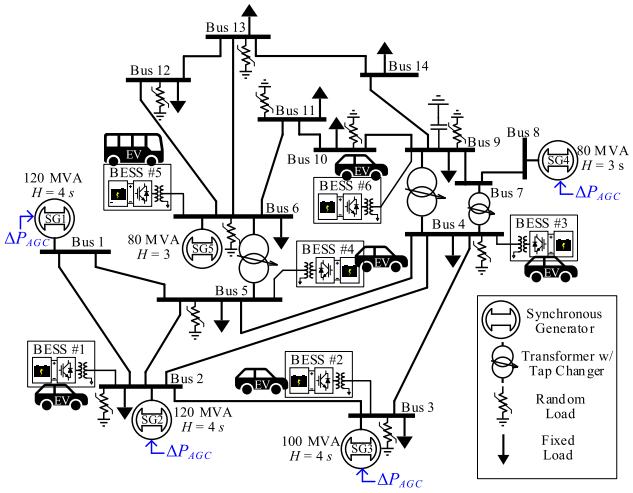

FIGURE 3. Modified IEEE 14-Bus system.

assuming that they originally used to charge the EVs at the rapid charging stations. The total capacity of the six BESSs is 3.0 MW, which is approximately 1.2% of the total average load.

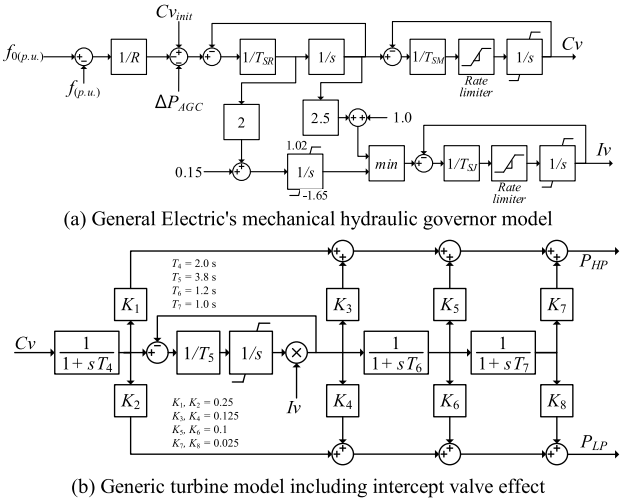

(a) General Electric's mechanical hydraulic governor model

(b) Generic turbine model including intercept valve effect

FIGURE 4. The governor and turbine model [33].

TABLE 1. Parameters of governor and turbine models.

Symbol	Quantity
f_0 , f	nominal SG and turbine frequency
R	frequency droop gain (0.05 p.u.)
$C_{v_{init}}$	control valve initial position in per unit
ΔP_{AGC}	power adjustment signal from the Secondary control
T_{SR} , T_{SM}	time constants of the speed relay and servo piston
C_v, I_v	governor output signals for turbine control valve and intercept control valve
P_{HP} , P_{LP}	mechanical output of high-pressure and low-pressure turbine
K_1~K_8	contributions to mechanical power of various turbine sections
T_4~T_7	time constants for the high-pressure turbine blow, the reheater, the crossover, and the double reheat unit

All synchronous generators in the modified IEEE 14-bus system are assumed to be steam turbine generators. For the governor, the mechanical hydraulic control model [33] is used (see FIGURE 4) and its parameters are listed in Table 1. The droop and dead bands in the governor response are set to 5% and 36 mHz, respectively. FIGURE 5 shows the AGC's logic diagram to generate the power reference of each synchronous generator (ΔP_{AGC}). In this paper, the AGC generates the control signal at every 4 s and is deactivated if Δf exceeds $\pm$200 mHz, as mentioned in [15]. K_{iAGC} and K_{pAGC} in FIGURE 5 are set to 0.336 and 3.0, respectively. Table 2 shows the detailed controller gains and power capacities on the EV charging BESSs.

TABLE 2. Parameters for the BESS and FR controller.

Symbol	Quantity	Value
P_{BESS}^{max}	power rating	500 kVA
α	contribution factor	0~1
SOC^{min},SOC^{max}	allowable range of SOC	10~90%
K_{pFR}	proportional gain of FR controller	100
K_{iFR}	integral gain of FR controller	10e3
K_{pI}	proportional gain of current controller	0.1
K_{iI}	integral gain of current controller	1e2
K_{pPLL}	PLL proportional gain	25
K_{iPLL}	PLL integral gain	355

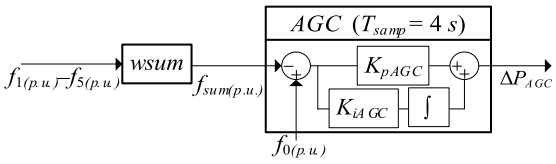

$f_{1(\text{p.u.}),\cdots,}f_{5(\text{p.u.})}$: Frequencies of five SGs (SG1 to SG5) in per unit.
$f_{sum(p.u.)}$: Weighted sum of the five SGs frequencies in per unit.
$f_{0(\text{p.u.})}$: Nominal frequency in per unit.
K_{pAGC}, K_{iAGC}: Proportional and integral gains of AGC.
ΔP_{AGC}: An AGC output signal distributed to each SG.

FIGURE 5. AGC logic.

IV. STABILITY ANALYSIS

The proposed FR controller (4) will provide the power reference P_{BESS}^{*} for the BESS, and the current reference (i_d^*, i_q^*) of the battery inverter is computed based on P_{BESS}^{*} using (8). To ensure the stable tracking of the actual current to the assigned reference, the PI current controller and the PLL gains are selected based on the impedance-based stability analysis in [34]. The small-signal impedance model [34] of the grid-connected inverter with the consideration of both the PLL gains and the current controller gains is used. This small- signal current model of inverter and grid system can be described as:

$$I_g(s) = \left[I_{inv}(s) - \frac{V_g(s)}{Z_{inv}(s)} \right] \frac{1}{1 + Z_g(s)/Z_{inv}(s)} \quad (9)$$

where (V_g, I_g) are the grid voltage and current, I_{inv} is the inverter current, Z_g and Z_{inv} are the grid and inverter impedances, respectively. It is assumed that the inverter can operate properly with the ideal grid, i.e. $Z_g = 0$. To stabilize the system (9) under the non-zero grid impedance, the inverter impedance should be designed so that the ratio Z_g/Z_{inv} satisfies the Nyquist stability criterion. In this paper, the grid impedance Z_g is measured in the PSCAD simulation of the modified IEEE 14-bus system using the current injection method in [35]. Instead of a simple L-filter in [34], an LCL-filter is used after the battery inverter. The inverter impedances with three different integral gain K_{iI} are plotted with the measured grid impedance in FIGURE 6. The inverter impedances intersect with the measured grid impedance at two different frequencies, i.e. at Point 1 (3Hz) and Point 2 (1203Hz). At Point 1, the phase margin is positive as PM=80deg, which indicating the stable condition. Around Point 2, only the inverter impedance with $K_{iI} = 1e4$ intersects with the measured grid impedance and the phase margin at this point is negative, i.e. PM $= -123$deg in FIGURE 6(c-d). This indicates the instability of the grid-connected inverter, which is then occurred in the current control simulation when the integral gain K_{iI} is changed from 1e3 to 1e4 in FIGURE 7.

V. SIMULATION STUDIES

This section investigates the effectiveness of the proposed FR scheme under various operating scenarios. The six BESSs in FEVCS autonomously operate, relying on the frequency measured at each terminal. This study analyzes the effect of EV charging BESS on the grid frequency and EV owners according to allocated FR power by adjusting α while performing charging mission. The operation modes can be described using four representative cases of α that can represent the most cases. The α values selected here are '$\alpha = 0$', '$\alpha = 0.3$', '$\alpha = 0.7$' and '$\alpha = 1$' when EV charging demands are 0.7 p.u. of the total BESS power. In the '$\alpha = 0$' mode, the BESSs only provide the charging services and do not assign power for FR. When '$\alpha = 1$', the entire BESS power is assigned for FR regardless of the EV charging demand. In this case, if the BESS is charging the EV, the FR power passing to the system is increased as much as possible by reducing the EV charging power. Conversely, when it is necessary to absorb power from the grid, EV and BESS will absorb power. The FR power has the highest priority for the BESS power utilization and the EVCS output power, P_{EVCS}, strictly follows the FR command in any FR mode ($\alpha > 0$). To achieve this, one assumption for the EV chargers is that EV charging power can be dynamically reduced from the demand level and restored back to that level immediately when needed. As a result, the EV charging pattern becomes discontinuous and pulsating, and the EV owners may get a longer EV charging time, but users may be able to participate in the FR service to save on charging costs.

For $0 < \alpha \leq 1$, it means that power is allocated according to the BESS maximum output rating. That is, $\alpha = 0.3$ means

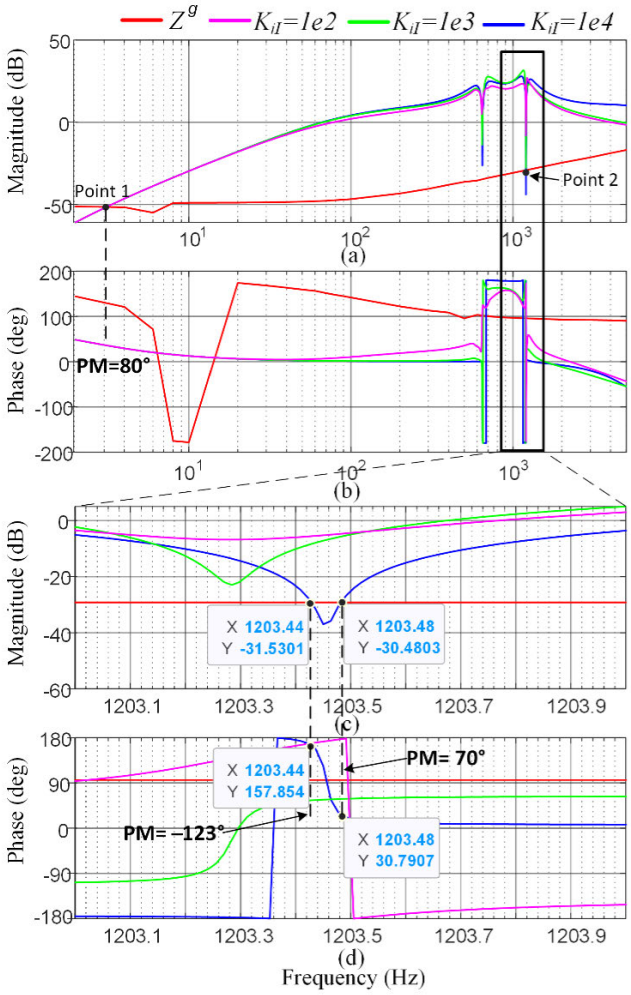

FIGURE 6. Bode plot of measured grid impedance and designed inverter impedance in d-q channel with different PI current controller gains.

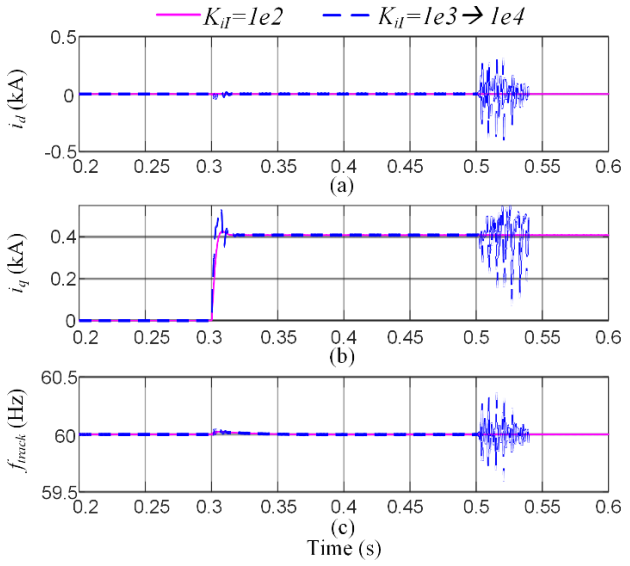

FIGURE 7. Current control performance with different PI controller gains. (a) (b) grid-side current in dq frame. (c) the estimated frequency from PLL.

that ±30% of P_{BESS}^{MAX} is the upper and lower power limit of FR. The number 0.3 for α is chosen because it is the maximum value of FR power that does not affect EV charging in a situation where the EV consumes 0.7 p.u. of BESS power in this assumed simulation condition. In another case, $\alpha = 0.7$ is selected as the one of representative cases in which the FR requirement affects the EV charging condition.

There are two main case studies are provided. Case I deals with the autonomous FR performance for the modified IEEE 14-bus system exposed to random load variations. In addition, as all BESSs are relying on the PLL-based local frequency measurement, the performance of the PLL is also an important factor for FR. In Case II, the performance evaluation is done for different PLL control bandwidths. For all cases, at t = 0 s, the total load starts to fluctuate, and the six BESSs start operation. For all cases, the initial SOCs of BESS1, BESS2, …, and BESS6 are set to 70%, 65%, 60%, …, 45%, respectively.

A. CASE I: AUTONOMOUS FR PERFORMANCE

FIGURE 8 shows the results when EV charging demand is less than the maximum power limit of the BESS. In this case, the EV charging demand is set to 0.7 p.u. of the BESS power limit. Beyond different α values to be compared, the load applied in the modified IEEE 14-bus system is the fixed load of 259 MW and an arbitrarily varying load within ±5 MW (2% of the total load) throughout the simulation. The total load continuously fluctuates as shown in FIGURE 8(a). As a result, FIGURE 8(b) shows how the fluctuation of the EPS frequency that changes with different α values. By changing α, the amount EV charging power can be adjusted.

For $\alpha = 0$, the entire EV charging power comes from the BESSs and no FR power exchange with the grid is seen. For $\alpha = 0.3$, the given EV charging demand becomes 0.7 p.u., Thus, the rest of the BESS power can be used for FR. In this case, 30% of the BESS power suppresses the frequency deviation and the probabilities for Δf within ±36 mHz increases to 68.2% from 51.5% (see FIGURE 6(c)). When $1 \geq \alpha > 0.3$, the FR power range can be retained by reducing the EV charging amount. It means that the sum of the EV demand and charging BESS power becomes P_{BESS}^{min} when over-frequency condition ($f > f_0$) and it becomes P_{BESS}^{max} when under-frequency mode ($f < f_0$). Evidently, the higher the amount of FR power, the better the frequency quality. The probabilities for Δf within ±36 mHz for $\alpha = 0.7$ and $\alpha = 1$ are 89.4% and 95.5%, respectively (see FIGURE 8(c)).

FIGURE 8(d)–8(f) shows the sum of the output powers of all BESSs, the sum of all EVCS side powers (the total FR power) and the total EV charging power, respectively. EV charging and FR power are not related if the sum of the FR power and EV charging power does not exceed 1 p.u.

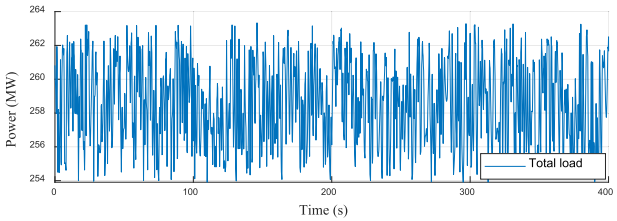

(a) Total load

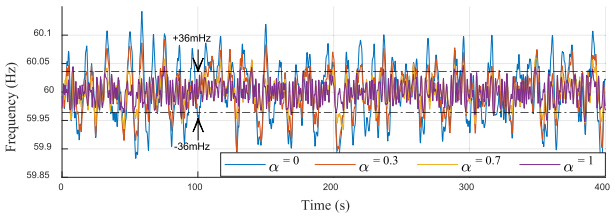

(b) Grid frequencies for different contribution factor α.

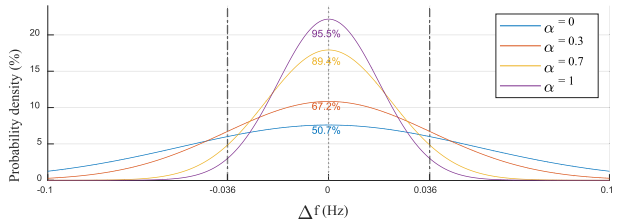

(c) Normal distribution curves for Δf

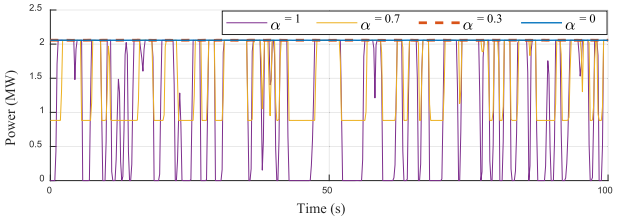

(d) Total sum of EV charging power with various α

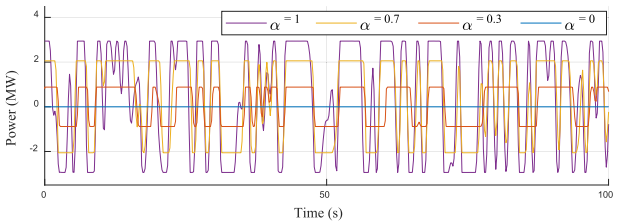

(e) Total sum of EVCSs' powers with various α

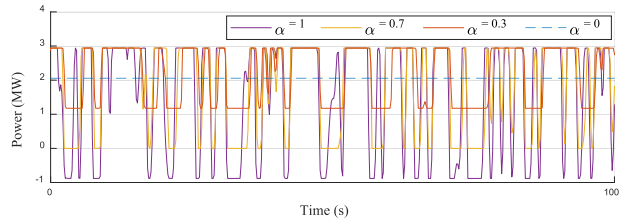

(f) Total sum of BESSs' output powers with various α

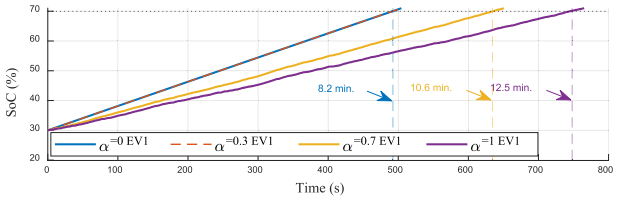

(g) EV Charging speed comparisons

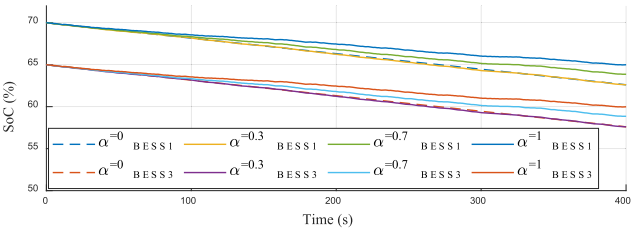

(h) SOCs of the BESS #1 and BESS #3 in the different EV loads

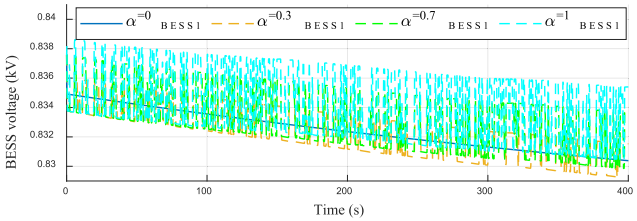

(i) Voltage profile of the BESS #1 with different factor α

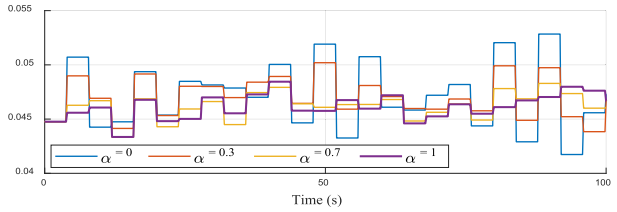

(j) AGC signal

FIGURE 8. **Results for Case I.**

As a result, the averages of the BESS outputs are almost identical as shown in FIGURE 8(f) (see $\alpha = 0$ and $\alpha = 0.3$). It is due to the FR power that we are considering is high frequency component without DC bias and it is related to AGC. No matter how random the load shakes the frequency, the long-term average value of the grid frequency can be maintained to the nominal value thanks to the AGC. In other words, the long-term summation of the injected/absorbed FR powers at each FEVCS are almost the same and has no DC bias.

Things get a bit complicated when $\alpha > 0.3$. The EV charging power starts to decrease from the original charging level (see FIGURE 8(d) $\alpha = 0.7$, $\alpha = 1$). As a result, the FR power increases above 0.3 p.u. of the maximum power. Eventually, the FR power can reach to the maximum power of the BESS (see FIGURE 8(e) $\alpha = 1$). Finally, for all α values, the BESSs output power varying ranges are determined as in FIGURE 8(f). The maximum becomes 1 p.u., and the minimum becomes –0.3 p.u. by considering 0.7 p.u. of the EV charging demand.

As mentioned earlier, the EV users have the disadvantage of connecting the FR while charging the EV, resulting in delays in charging time. FIGURE 8(g) compares how the EV charging time varies with different α values. As the test condition, for each EVCS, it is assumed that an approximately 100 kWh vehicle is being charged by a super-fast charging (350 kW). FIGURE 6(g) shows how the initial SoC of EV1 in EVCS #1 rises. The initial EV SOC is 30% and the target SOC is 70%. As can be seen, $\alpha = 0$ and $\alpha = 0.3$ conditions show superimposed straight SOC lines with a charging time of 8.2 min. For $\alpha = 0.7$, the charging time is delayed by 29.2%, and under the full FR condition ($\alpha = 1$), the total charging takes 12.5 minutes, which takes 152.4% of the time compared to the condition without FR.

From the EV borrower's point of view, the charging time is partially increased in return for participating in FR. In contrast, from the EVCS owner's point of view, the effect of sharing a portion of EV charging power to the system during FR can be expected. As shown in Fig. 8(h), as the FR participation rate increases, it can be seen that the amount of battery energy consumed for EV charging in BESS1 and BESS3 decreases (it applies to all BESSs in the EPS). Based on the 500kWh battery, it has the effect of preventing the consumption of SOC by 2.5% for approximately 400 seconds.

FIGURE 8(j) shows the AGC control signal for all SGs in the EPS. During the control period of 4 sec, AGC generates its power correction signals (ΔP_{AGC}). Obviously, Δf affects the AGC output due to the FR support of the autonomous BESSs. In addition, the variation range of the AGC signal is significantly reduced by increasing the participating factor α.

As the considered system in FIGURE 3 above, there are 6 EVCSs connected to the 14-bus power system with five synchronous generators. The total power flows for generation, load, EVCS, EV and BESS are shown in FIGURE 9. At 50 seconds, the load power will start to have fluctuated powers at 11 buses in the 14-bus power system. Before that, only fixed load is added in the simulation. The total generation power from five SGs, the total load power and the total power of six EVCSs are denoted as P_{gen}, P_{load} and P_{evcs} in FIGURE 9(a) and 9(b). Due to the small value of EVCS power compared with generator and load powers, the power sum of P_{evcs} and P_{gen} are used to represent the contribution of EVCS power as the red solid line in FIGURE 9(b).

It is difficult to justify the effectiveness of the proposed FR by evaluating the power flows in FIGURE 9(a-b). Therefore, the power mismatches between generation and load powers are shown in FIGURE 9(c). This power mismatch in two cases with FR and without FR are plotted as the red and blue solid line in FIGURE 9(d). The mismatch levels in the two cases are similar, but the peak value of the case with FR is larger than that without FR. Under the continuous variation of load disturbance, the larger power difference results in a better frequency performance as shown in FIGURE 9(d). The

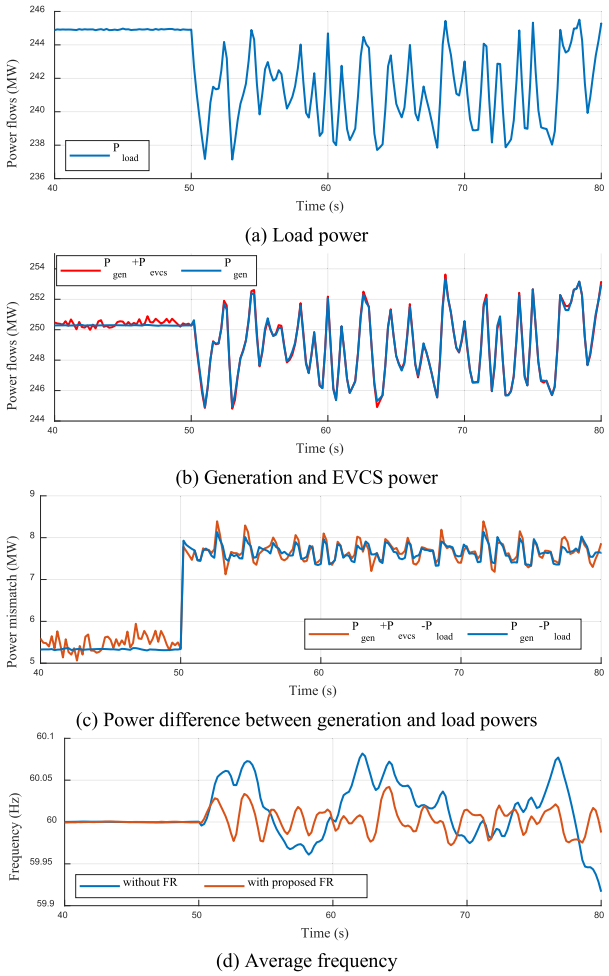

FIGURE 9. Results of total generation, EVCS and load power differences without FR (blue solid line) and with FR (red solid line).

frequency deviation with the proposed FR is almost twice smaller than that without FR.

B. CASE II: EFFECTS OF THE PLL BANDWIDTHS

As the BESS purely relying on the PLL for grid frequency estimation, and it may impact the FR performance when different bandwidths are used from the various power converter vendors. The PLL bandwidth in Table 2 is default value given in PSCAD, which is equivalent to the one-fifth of the line frequency f_0, roughly.

To obtain detailed information about the effect of PLL, it is compared with four different bandwidths of the BESS PLL. That is, one-fifth, 1/20, 1/40 and 1/100 of the line frequency ($f_0 = 60Hz$). The default PLL parameters given in Table 2 are provided for the PSCAD inherent setting and it is equivalent to one-fifth of f_0. In the typical applications, a more conservative gain is used which may create 1/20 of f_0 [36]. As an extreme case, 1/100 bandwidth is simulated for the worst-case scenario.

As shown in FIGURE 10, the FR performances are compared in the case of $\alpha = 1$. The performance is almost identical except for the very slight performance improvement

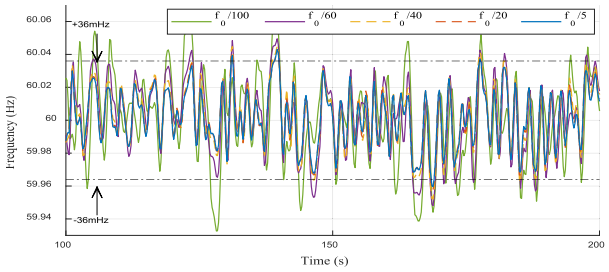

(a) Grid frequencies for different PLL control bandwidth

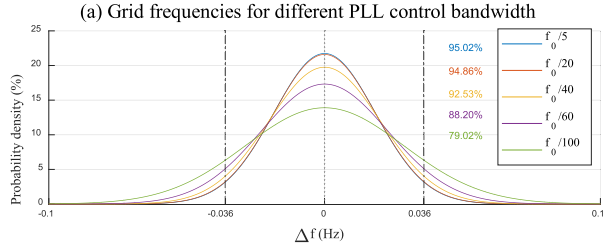

(b) Normal distribution curves for Δf

FIGURE 10. **FR performance w.r.t the PLL bandwidth.**

when the bandwidth is as low as 1/20 of f_0. However, when the bandwidth is lower than 1/40 of the line frequency, the FR performance deterioration becomes obvious. This may be because the FR frequency to which the BESS responds and the PLL bandwidth are adjacent to each other, and the coupling effect between the PLL and the grid frequency begins to appear.

VI. CONCLUSION

This paper proposes an autonomous FR scheme using the dedicated BESSs for EV charging. The BESSs estimates the grid frequency from the measured voltages at the terminal. The proposed scheme adjusts the power from the BESS and EV in association with the estimated frequency deviation.

Simulation results clearly demonstrate that the BESSs with a small portion of the total load can significantly mitigate the frequency fluctuations caused by the continuously varying loads. In addition, the effects of the PLL bandwidths on the performance of the proposed scheme is investigated.

The advantage of the proposed autonomous FR scheme is that it can improve the EPS flexibility without additional devices in a cost-effective way. Thus, from the EPS operator's viewpoint, more flexibility resources autonomously responding the frequency deviation are secured. In addition, from the FEVCS's viewpoint, the income will increase by being paid by providing the grid services. Finally, the proposed FR scheme can help maintain the frequency deviation within a narrow band in the EPS that has a high variable renewable generation resources.

REFERENCES

[1] M. O. Metais, O. Jouini, Y. Perez, J. Berrada, and E. Suomalainen, "Too much or not enough? Planning electric vehicle charging infrastructure: A review of modeling options," *Renew. Sustain. Energy Rev.*, vol. 153, Jan. 2022, Art. no. 111719.

[2] N. Kumar, T. Kumar, S. Nema, and T. Thakur, "A multiobjective planning framework for EV charging stations assisted by solar photovoltaic and battery energy storage system in coupled power and transportation network," *Int. J. Energy Res.*, vol. 46, no. 4, pp. 4462–4493, Mar. 2022.

[3] O. Hafez and K. Bhattacharya, "Optimal design of electric vehicle charging stations considering various energy resources," *Renew. Energy*, vol. 107, pp. 576–589, Jul. 2017.

[4] X. Li, D. Hui, and X. Lai, "Battery energy storage station (BESS)-based smoothing control of photovoltaic (PV) and wind power generation fluctuations," *IEEE Trans. Sustain. Energy*, vol. 4, no. 2, pp. 464–473, Apr. 2013.

[5] A. Hussain, V.-H. Bui, J.-W. Baek, and H.-M. Kim, "Stationary energy storage system for fast EV charging stations: Optimality analysis and results validation," *Energies*, vol. 13, no. 1, p. 230, Jan. 2020.

[6] D. Sbordone, I. Bertini, B. D. Pietra, M. C. Falvo, A. Genovese, and L. Martirano, "EV fast charging stations and energy storage technologies: A real implementation in the smart micro grid paradigm," *Electr. Power Syst. Res.*, vol. 120, pp. 96–108, Mar. 2015.

[7] R. Varma, T. Hartley, S. Mohan, A. Royal, F. Sara, D. Sarin, and S. Williams, "Utility energy savings by novel smart inverter control of PV systems, BESS and EV charging stations as statcoms," in *Proc. CIGRE Canada Conf.*, 2020, pp. 1–9.

[8] J. Zhong, L. He, C. Li, Y. Cao, J. Wang, B. Fang, L. Zeng, and G. Xiao, "Coordinated control for large-scale EV charging facilities and energy storage devices participating in frequency regulation," *Appl. Energy*, vol. 123, pp. 253–262, Jun. 2014.

[9] A. Ovalle, A. Hably, S. Bacha, and M. Ahmed, "Voltage support by optimal integration of plug-in hybrid electric vehicles to a residential grid," in *Proc. 40th Annu. Conf. IEEE Ind. Electron. Soc. (IECON)*, Oct. 2014, pp. 4430–4436.

[10] K. Dhingra and M. Singh, "Frequency support in a micro-grid using virtual synchronous generator based charging station," *IET Renew. Power Gener.*, vol. 12, no. 9, pp. 1034–1044, Jul. 2018.

[11] N. Jaleeli, L. S. VanSlyck, D. N. Ewart, L. H. Fink, and A. G. Hoffmann, "Understanding automatic generation control," *IEEE Trans. Power Syst.*, vol. 7, no. 3, pp. 1106–1122, Aug. 1992, doi: 10.1109/59.207324.

[12] R. K. Green, "Transformed automatic generation control," *IEEE Trans. Power Syst.*, vol. 11, no. 4, pp. 1799–1804, Nov. 1996.

[13] D. C. H. Prowse, "Improvements to a standard automatic generation control filter algorithm," *IEEE Trans. Power Syst.*, vol. 8, no. 3, pp. 1204–1210, Aug. 1993.

[14] A. Ulbig, M. D. Galus, S. Chatzivasileiadis, and G. Andersson, "General frequency control with aggregated control reserve capacity from time-varying sources: The case of PHEVs," in *Proc. IREP Symp. Bulk Power Syst. Dyn. Control VIII (IREP)*, Aug. 2010, pp. 1–14.

[15] J. Machowski, Z. Lubosny, J. W. Bialek, and J. R. Bumby, *Power System Dynamics: Stability and Control*, 3rd ed. Hoboken, NJ, USA: Wiley, 2020.

[16] D. Kottick, M. Blau, and D. Edelstein, "Battery energy storage for frequency regulation in an island power system," *IEEE Trans. Energy Convers.*, vol. 8, no. 3, pp. 455–459, Sep. 1993.

[17] C.-F. Lu, C.-C. Liu, and C.-J. Wu, "Effect of battery energy storage system on load frequency control considering governor deadband and generation rate constraint," *IEEE Trans. Energy Convers.*, vol. 10, no. 3, pp. 555–561, Sep. 1995.

[18] B. Xu, A. Oudalov, J. Poland, A. Ulbig, and G. Andersson, "BESS control strategies for participating in grid frequency regulation," *IFAC Proc. Volumes*, vol. 47, no. 3, pp. 4024–4029, 2014.

[19] D.-I. Stroe, V. Knap, M. Swierczynski, A.-I. Stroe, and R. Teodorescu, "Operation of a grid-connected lithium-ion battery energy storage system for primary frequency regulation: A battery lifetime perspective," *IEEE Trans. Ind. Appl.*, vol. 53, no. 1, pp. 430–438, Jan. 2017.

[20] Y. J. A. Zhang, C. Zhao, W. Tang, and S. H. Low, "Profit-maximizing planning and control of battery energy storage systems for primary frequency control," *IEEE Trans. Smart Grid*, vol. 9, no. 2, pp. 712–723, Mar. 2018.

[21] H. Liu, Z. Hu, Y. Song, and J. Lin, "Decentralized vehicle-to-grid control for primary frequency regulation considering charging demands," *IEEE Trans. Power Syst.*, vol. 28, no. 3, pp. 3480–3489, Aug. 2013.

[22] M. M. Mahfouz and R. Iravani, "A supervisory control for resilient operation of the battery-enabled DC fast charging station and the grid," *IEEE Trans. Power Del.*, vol. 36, no. 4, pp. 2532–2541, Aug. 2021.

[23] X.-G. Yang, G. Zhang, S. Ge, and C.-Y. Wang, "Fast charging of lithium-ion batteries at all temperatures," *Proc. Nat. Acad. Sci. USA*, vol. 115, no. 28, pp. 7266–7271, Jul. 2018.
[24] Z. Tan, X. Li, L. He, Y. Li, and J. Huang, "Primary frequency control with BESS considering adaptive SoC recovery," *Int. J. Electr. Power Energy Syst.*, vol. 117, May 2020, Art. no. 105588.
[25] H.-S. Kim, J. Hong, and I.-S. Choi, "Implementation of distributed autonomous control based battery energy storage system for frequency regulation," *Energies*, vol. 14, no. 9, pp. 1–19, 2021.
[26] K. Doenges, I. Egido, L. Sigrist, E. L. Miguélez, and L. Rouco, "Improving AGC performance in power systems with regulation response accuracy margins using battery energy storage system (BESS)," *IEEE Trans. Power Syst.*, vol. 35, no. 4, pp. 2816–2825, Jul. 2020.
[27] Y.-J. Kim, G. Del-Rosario-Calaf, and L. K. Norford, "Analysis and experimental implementation of grid frequency regulation using behind-the-meter batteries compensating for fast load demand variations," *IEEE Trans. Power Syst.*, vol. 32, no. 1, pp. 484–498, Jan. 2017.
[28] N. S. E. Guzman, C. A. Cañizares, K. Bhattacharya, and D. Sohm, "Frequency regulation model of bulk power systems with energy storage," *IEEE Trans. Power Syst.*, vol. 37, no. 2, pp. 913–926, Mar. 2022.
[29] Y. Ota, H. Taniguchi, T. Nakajima, K. M. Liyanage, K. Shimizu, T. Masuta, J. Baba, and A. Yokoyama, "Autonomous distributed vehicle-to-grid for ubiquitous power grid and its effect as a spinning reserve," *J. Int. Council Electr. Eng.*, vol. 1, no. 2, pp. 214–221, Apr. 2011.
[30] R. Sharma, A. Zakerian, and M. Karimi-Ghartemani, "Local controller for an autonomous grid-supportive battery energy storage system," *IEEE Trans. Power Electron.*, vol. 37, no. 2, pp. 2191–2202, Feb. 2022.
[31] Y. Ota, H. Taniguchi, T. Nakajima, K. M. Liyanage, J. Baba, and A. Yokoyama, "Autonomous distributed V2G (vehicle-to-grid) satisfying scheduled charging," *IEEE Trans. Smart Grid*, vol. 3, no. 1, pp. 559–564, Mar. 2012.
[32] F. Blaabjerg, R. Teodorescu, M. Liserre, and A. V. Timbus, "Overview of control and grid synchronization for distributed power generation systems," *IEEE Trans. Ind. Electron.*, vol. 53, no. 5, pp. 1398–1409, Oct. 2006.
[33] F. P. Mello, P. Anderson, J. Doudna, J. H. Fish, and P. A. L. Hamm, "Dynamic models for fossil fueled steam units in power system studies," *IEEE Trans. Power Syst.*, vol. 6, no. 2, pp. 753–761, May 1991.
[34] B. Wen, D. Boroyevich, R. Burgos, P. Mattavelli, and Z. Shen, "Analysis of D-Q small-signal impedance of grid-tied inverters," *IEEE Trans. Power Electron.*, vol. 31, no. 1, pp. 675–687, Jan. 2016.
[35] G. Francis, R. Burgos, D. Boroyevich, F. Wang, and K. Karimi, "An algorithm and implementation system for measuring impedance in the D-Q domain," in *Proc. IEEE Energy Convers. Congr. Expo.*, Sep. 2011, pp. 3221–3228.
[36] K. Sharifabadi, L. Harnefors, H. Nee, S. Norrga, and R. Teodorescu, *Design, Control and Application of Modular Multilevel Converters for HVDC Transmission Systems*. Hoboken, NJ, USA: Wiley, 2016.

CHANGWOO YOON (Member, IEEE) received the B.S. and M.S. degrees in electrical engineering from the Seoul National University of Science and Technology (SeoulTech), Seoul, South Korea, in 2007 and 2009, respectively, and the Ph.D. degree from the Energy Technology Program, Aalborg University, Aalborg, Denmark, in 2017.

He was a Hardware Design Engineer with Advance Drive Technology, Anyang, South Korea, from 2009 to 2013. In 2015, he was a Visiting Scholar at the University of Manitoba, Canada. And, he was with Rolls-Royce Corporate Laboratory, NTU, Singapore, as a Research Fellow, from 2017 to 2018. He was a Senior Engineer with Xnergy Autonomous Power Technology, Singapore, in 2019. Since 2020, he has been working as a Research Professor with the Research Center of Electrical and Information Technology (RCEIT), SeoulTech. His main research interest includes modeling and control of power electronics-based systems. He was a recipient of the IEEE Industry Applications Society Third Prize Paper Award, in 2019.

NGOC-DUC NGUYEN received the B.Sc. degree in mechatronics from the Ho Chi Minh University of Technology, in 2014, and the M.S. and Ph.D. degrees in control engineering from Korea Maritime and Ocean University, South Korea, in 2016 and 2019, respectively.

He has worked as a Research Professor at the Research Center for Electrical and Information Technology, Seoul National University of Science and Technology. His research interests include automatic control and its implementation in robotics, electrical machines, power converters, and hybrid batteries.

YONG CHEOL KANG (Senior Member, IEEE) received the B.S., M.S., and Ph.D. degrees in electrical engineering from Seoul National University, Seoul, South Korea, in 1991, 1993, and 1997, respectively. From 1999 to 2017, he was a Professor at the Department of Electrical Engineering, Chonbuk National University, Jeonju, South Korea. He was the Director of the WeGAT Research Center supported by the MSIP, South Korea. Since 2018, he has been with Yonsei University, Seoul. His research interests include the development of control and protection techniques for wind turbine generators and wind power plants. He is a member of the International Electrotechnical Commission Working Group TC88/WG27 and an Editor of IEEE TRANSACTIONS ON SUSTAINABLE ENERGY.

YOUNG-IL LEE (Senior Member, IEEE) received the B.S., M.S., and Ph.D. degrees in control and instrumentation engineering from Seoul National University (SNU), in 1986, 1988, and 1994, respectively.

He was a Visiting Research Fellow at the Department of Engineering Science, Oxford University, from February 1998 to July 1999 and from February 2007 to July 2007. He worked with Gyeongsang National University, from 1994 to 2001, and moved to Seoul National University of Science and Technology (SeoulTech), in 2001. He is currently a Professor at the Department of Electrical and Information Engineering, SeoulTech. Currently, he is the Director of the Electrical Vehicle Society, Korea Institute of Electrical Engineering (KIEE), and the Head of the Research Center of Electrical and Information Technology, SeoulTech. His scientific research interests include MPC for systems with input constraints and model uncertainties, MPC method for dc–dc, ac–dc converter and dc–ac inverter, control of EV chargers, control of ac motors for EV application, and energy management algorithm of micro-grids. He served as an Editor for *International Journal of Control, Automation and Systems* (IJCAS) and *International Journal of Automotive Technology* (IJAT), from 2017 to 2019, respectively.